ARMY RESEARCH LABORATORY

ARL

A Preliminary Investigation of Traumatically Induced Axonal Injury in a Three-Dimensional (3-D) Finite Element Model (FEM) of the Human Head During Blast-Loading

by Amy M. Dagro, Philip J. McKee, Reuben H. Kraft, Timothy G. Zhang, and Sikhanda S. Satapathy

NOTICES

Disclaimers

Army Research Laboratory

Aberdeen Proving Ground, MD 21005-5069

A Preliminary Investigation of Traumatically Induced Axonal Injury in a Three-Dimensional (3-D) Finite Element Model (FEM) of the Human Head During Blast-Loading

Amy M. Dagro and Sikhanda S. Satapathy
Weapons and Materials Research Directorate, ARL

Philip J. McKee
Dynamic Science, Inc.

Reuben H. Kraft
**The Pennsylvania State University Department of Mechanical
and Nuclear Engineering**

Timothy G. Zhang
Bowhead Science and Technology

REPORT DOCUMENTATION PAGE

Form Approved OMB No. 0704-0188

1. REPORT DATE (DD-MM-YYYY)	2. REPORT TYPE	3. DATES COVERED (From - To)
July 2013	Final	May 2012–May 2013

4. TITLE AND SUBTITLE

A Preliminary Investigation of Traumatically Induced Axonal Injury in a Three-Dimensional (3-D) Finite Element Model (FEM) of the Human Head During Blast-Loading

5a. CONTRACT NUMBER

5b. GRANT NUMBER

5c. PROGRAM ELEMENT NUMBER

6. AUTHOR(S)

Amy M. Dagro, Philip J. McKee,[*] Reuben H. Kraft,[†] Timothy G. Zhang,[‡] Sikhanda S. Satapathy

5d. PROJECT NUMBER

5e. TASK NUMBER

5f. WORK UNIT NUMBER

7. PERFORMING ORGANIZATION NAME(S) AND ADDRESS(ES)

U.S. Army Research Laboratory
ATTN: RDRL-WMP-B
Aberdeen Proving Ground, MD 21005-5069

8. PERFORMING ORGANIZATION REPORT NUMBER

ARL-TR-6504

9. SPONSORING/MONITORING AGENCY NAME(S) AND ADDRESS(ES)

10. SPONSOR/MONITOR'S ACRONYM(S)

11. SPONSOR/MONITOR'S REPORT NUMBER(S)

12. DISTRIBUTION/AVAILABILITY STATEMENT

Approved for public release; distribution is unlimited.

13. SUPPLEMENTARY NOTES

[*]Dynamic Science, Inc., 1003 Old Philadelphia Rd., Ste. 210, Aberdeen, MD 21001
[†]The Pennsylvania State University Department of Mechanical & Nuclear Engineering, 137 Reber Building University Park, PA 16802
[‡]Bowhead Science and Technology, UIC Technical Services _____

14. ABSTRACT

In the context of recent military conflicts and the prevalence of improvised explosive devices (IEDs), there has been an eminent need to better understand the mechanisms of brain injury resulting from blast exposure of military personnel. In this study, Diffusion Tensor Imaging (DTI) was used to inform a human head finite element model (FEM) to create a transversely isotropic description of the white matter fiber tissue. For each element in the model that spatially occupied the same regions as the white matter fiber tractography, the strain was calculated in the direction of the axonal fiber bundles. The axonal strain was used to predict the prevalence of diffuse axonal injury in blast events. It was found that the presence of axonal strains above a critical threshold were widespread, and the maximal axonal strains in the white matter tissue occur long after (10–20 ms) the initial shock wave has been applied to the head. Maximum axonal strains and shear stress values were increased due to brain tissue deformation from head rotation.

15. SUBJECT TERMS

diffuse axonal injury (DAI), traumatic brain injury (TBI), blast TBI (bTBI), computational biomechanics of brain tissue, finite element model (FEM)

16. SECURITY CLASSIFICATION OF:			17. LIMITATION OF ABSTRACT	18. NUMBER OF PAGES	19a. NAME OF RESPONSIBLE PERSON Amy M. Dagro
a. REPORT	b. ABSTRACT	c. THIS PAGE			19b. TELEPHONE NUMBER (Include area code)
Unclassified	Unclassified	Unclassified	UU	30	(410) 278-3889

Standard Form 298 (Rev. 8/98)
Prescribed by ANSI Std. Z39.18

Contents

List of Figures

List of Tables

Preface

This report is the result of a collaborative effort between government and contractor personnel. Amy M. Dagro (ARL) was responsible for running simulations and performing the majority of data analysis. Philip J. McKee of Dynamic Science, Inc. (DSI) was responsible for the creation of the finite element model (FEM) from magnetic resonance imaging (MRI) data and assisted with the data analysis. Reuben Kraft (PSU) was essential in the idea/concept of the work, and assisted with data analysis and conclusions. Sikhanda Satapathy (ARL) and Timothy Zhang (Bowhead Science and Technology) contributed to the analysis of applied and intracranial pressures from blast-loading.

Acknowledgments

1. Introduction

The possible mechanisms, by which traumatic brain injury (TBI) occurs during blast events, remain unclear. Blast-induced TBI is thought to be a direct consequence of the fast-moving pressure transient from the initial blast wave, and has been recognized as the signature wound in recent military conflicts (*1*). Current research has focused on blast-induced injury; however, the research has been primarily limited to animal and in vitro surrogates. Although this provides useful information on potential mechanisms, it may not be fully representative of the mechanical loading and response within the human brain. A second challenge in current blast TBI (bTBI) research is the limited understanding of the complex systemic response of multiple neurodegenerative molecular pathways (*2*).

A recent study of military personnel exposed to primary blast-related and "mild" TBI, but no other known insult, showed abnormalities in diffusion tensor magnetic resonance imaging (MRI) consistent with cerebellar white matter injury (*3*). The multifocal pathological finding of white matter disruption can be indicative of Diffuse Axonal Injury (DAI). The primary mechanism of axonal injury is deformation of brain tissue, which induces misalignment in the cytoskeletal network or changes to the axolemma permeability—inducing a cascade of subcellular events— ultimately leading to severance of the axon (*4*).

The structural organization of white matter in the brain can be captured in great detail with advanced diffusion magnetic resonance (MR) imaging schemes (*5*). The objective of this effort is to use a three-dimensional (3-D) finite element model (FEM) informed by Diffusion Tensor Imaging (DTI), to calculate strains in the direction of white matter fiber bundles, and then predict the amount of DAI that results from rotational head movement during a blast event.

In contrast to recent papers, which use FEM to predict changes to intracranial pressure during blast-loading (*6, 7, 8*), we will examine the brain's axonal strain from blast-loading, since it is known that DAI is prevalent in nonimpact coronal rotation (*9*).

2. Methods

2.1   Creation of the Finite Element Model

Wright and Ramesh (*10, 11*) have shown that the degree of predicted DAI in a computational model is highly dependent on the incorporation of axonal direction in the anisotropy of the constitutive model. The 3-D finite element human head model was constructed from MRI data (*12, 13*). The previously developed human head model was then attached to the geometry of a male body (open3dproject.org), and scaled so that the total height was 1.8 meters (m).

White matter fibers in the brain, which consist of axon bundles, are reconstructed from DTI data. An algorithm was previously developed by ARL to import diffusion-weighted imaging data (in this case, DTI data) into the volume elements, so that each element of the cerebral white matter is assigned an average vector representation of the orientation of white matter fibers that exist in that element (*14*). Simulations were performed with a Lagrangian, 3-D explicit, transient dynamics code and a nodal-based tetrahedral formulation to prevent the volumetric locking and stiffness associated with regular tetrahedral elements (*15*). The final FEM (figure 1) had 874,788 nodal-based tetrahedral elements, including 358,948 elements in the cerebrum and cerebellum. Simulations ran on 128 processors for approximately 68 h.
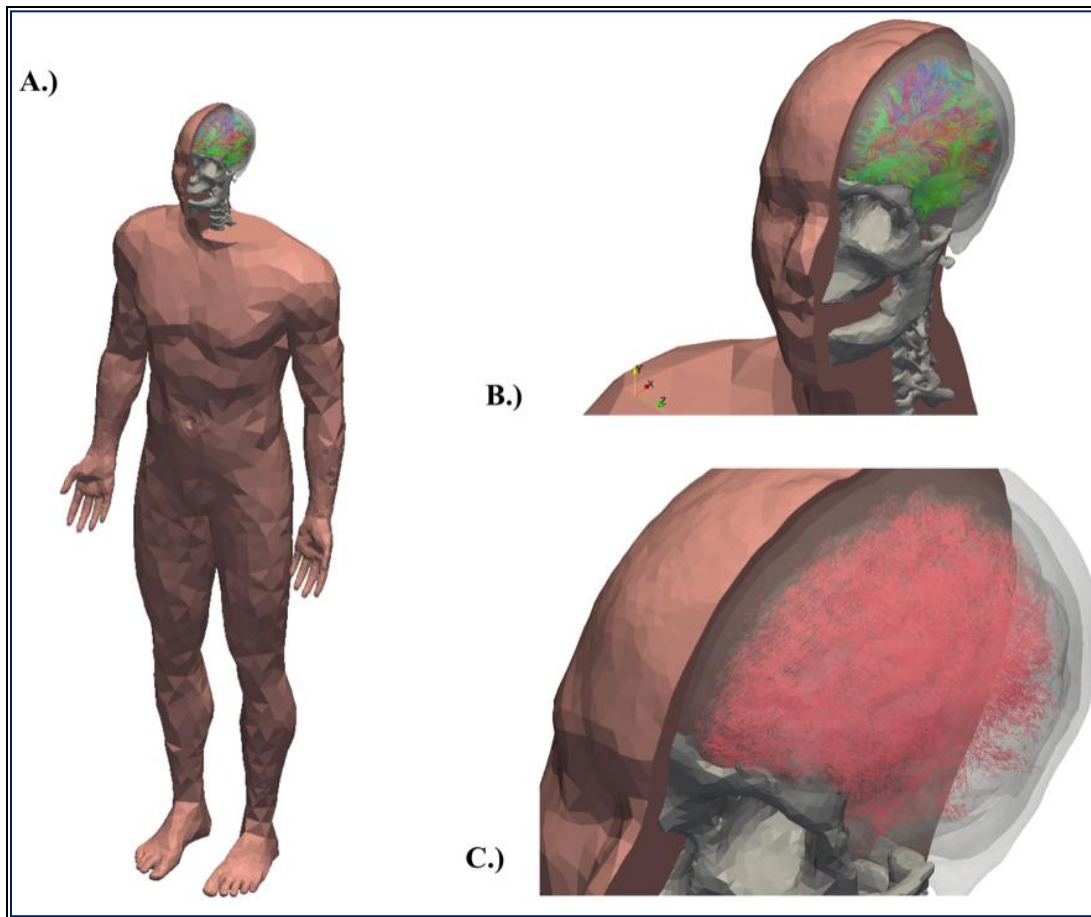
Figure 1. The FEM used in the study. A.) Finite element human body model with DTI fiber tractography; B.) Closeup of original DTI fiber tractography; C.) Vector representation of fiber directions assigned to each tetrahedral element in the FEM.

Neither tangential sliding, nor normal separations were allowed at any of the interfaces between tissues. The detailed geometry of the surface of the gray matter was included, since the presence of sulci alters the strain and strain distribution in the model (*16*).

2.2   Constitutive Models and Material Properties

Local brain motion is also highly sensitive to the shear properties of brain tissue (*17*). Recent studies have shown that previously accepted shear moduli of brain tissue were too large (*17, 18*). One advantage of incorporating the anisotropy of white matter is to account for axonal fiber bundles, reported to be up to three times stiffer than the surrounding matrix (*19*). A more detailed description of the transversely isotropic hyperlastic model, and the additional parameter C_3, which describes an exponential behavior in the fiber direction is available in Kraft et al. (14). The gray matter of the brain was treated as an isotropic material.

The material properties and constitutive models used are shown in table 1.

Table 1. FE model material properties.

	Material Model	**Material Properties**
Scalp/skin/fat/muscle	Elastic	$\rho = 1050$ kg/m^3 E = 1.67e7 Pa $\upsilon = 0.42$
Skull and vertebral bones	Elastic	$\rho = 2000$ kg/m^3 E = 6.0e9 Pa $\upsilon = 0.229$
Cerebrum and Cerebellum White Matter	Transversely Isotropic hyperelastic	$\rho = 1040$ kg/m^3 $C_{10} = 1500$ Pa $C_{01} = 1700$ Pa $C_3 = 2700$ Pa K = 2.1e9 Pa
Cerebrum and Cerebellum Gray Matter	Mooney-Rivlin hyperelastic	$\rho = 1040$ kg/m^3 $C_{10} = 1500$ Pa $C_{01} = 1700$ Pa K = 2.1e9 Pa
Brainstem	Viscoelastic Swanson	$G_\infty = 0.27$ $G_1 = 0.73$, $\tau_1 = 100$ s^{-1} $A_1 = B_1 = 4500$ Pa K = 1.72e9 Pa
Cerebrospinal Fluid, Ventricles	Mooney-Rivlin hyperelastic	$\rho = 1040$ kg/m^3 $C_{10} = 200$ Pa $C_{01} = 200$ Pa K = 2.2e9 Pa
Intervertebral discs	Viscoelastic Swanson[a]	$G_1 = 0.1392$, $\tau_1 = 0.001477$ s^{-1} $G_2 = 0.1587$, $\tau_2 = 0.0615$ s^{-1} $G_3 = 0.2234$, $\tau_3 = 1.017$ s^{-1} $G_4 = 0.4787$, $\tau_4 = 13.2$ s^{-1} $A_1 = B_1 = 2100$ Pa K = 1.72e9 Pa

[a]Prony terms of the viscoelastic Swanson model are normalized.

The transversely isotropic hyperelastic model also enabled the calculation of axonal strain. The axonal strain is defined as the engineering strain resolved in the direction of the original average fiber bundle direction that traverses the volume element (*20*). Axonal strain is calculated within the Sierra framework using the method outlined below.

The deformation gradient is given by:

$$F = \frac{dx}{dX}.$$

(1)

The extension ratio, λ, is calculated as:

$$\lambda_{axonal}{}^2 = \frac{dx^T \times dx}{dX^T \times dX} = \frac{dX^T}{dX^T \times dX} \times F^T \times F \times \frac{dX}{dX^T \times dX}$$

$$\lambda_{axonal}{}^2 = a^T \times F^T \times F \times a,$$

(2)

where **a** is the unit vector in the direction of axonal orientation. Since the extension ratio is the new length divided by the original length, the strain is given by:

$$\varepsilon_{axonal} = \lambda\text{-}1.$$

(3)

2.3 Applied Loading Conditions

The applied blast pressure was performed using the Presto Blast Function in the Sierra Solid Mechanics suite of codes (Sandia National Laboratories). The input parameters use Sach's scaling to match the empirical data from ConWep 2.1.0.8, which provides the incident and reflected pressures. The angle of incidence is accounted for by the following relationship (*21*):

$$P_{total} = P_{ref} * \cos\theta + P_{inc} * (1 - \cos\theta),$$

(4)

where θ is the angle between the direction to the blast and the face-normal-vector, P_{total} is the total pressure, P_{ref} is the reflected pressure at normal incidence, and P_{inc} is the incident pressure. Two simulations were performed: one where the head was allowed to rotate with the neck, and one with a free-boundary condition. For the applied pressure loading in both simulations, an equivalent of 5 lbs of TNT was detonated 3 m in front of the body at a midthoracic height. Effects of reflections from the ground or interfering objects are not captured in this Lagrangian simulation. This resulted in a frontal peak incident pressure of 210 kPa and a positive duration of 2.8 milliseconds (ms) (figure 2), which is survivable with ballistic protective body armor according to previously developed blast injury risk functions, and is also sufficiently below the 50% survivability limit for lethal head injury (*22*).

A fixed boundary condition was applied to the entirety of the body below the T1 vertebra, so that the head and neck were free to rotate, since mechanical loading to the torso is not within the scope of this analysis. A full homogenous body mass with skin-like material properties was included below the head-neck structures to simulate an accurate mitigation of the shock wave propagation into the brain, which may be relevant since the detonation point of the blast is located at an angle below the head.
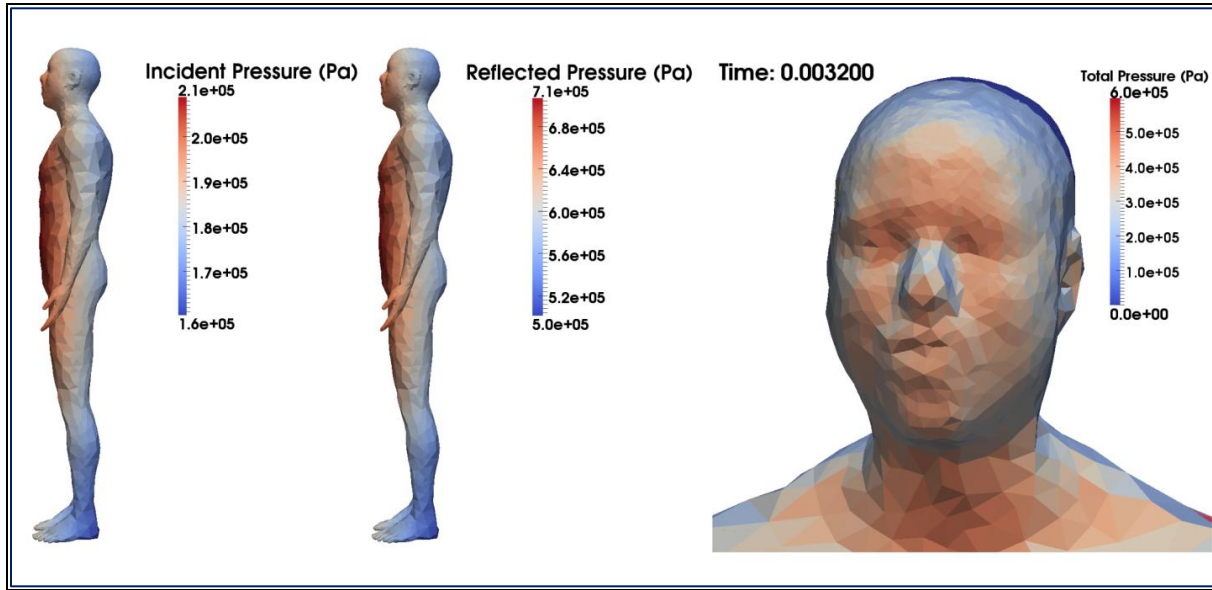
Figure 2. Calculated incident, reflected, and total pressures at the surface of the body.

3. Validation Efforts of the Model Against Impact and Acceleration Experiments

The pressure response of the model was compared to the cadaveric experimental data of Nahum et al. (23), where impacts to the forehead by a cylindrical padded impactor were performed. Bradshaw and Morfey (24) showed that it is insufficient to validate FE models for pressure since pressure validation alone does not account for accuracy in strain. Therefore, cadaveric tests showing local brain motions using an x-ray system and neutral density targets (NDTs) were used to validate the magnitude of peak brain displacements (25). A more detailed account of these validation efforts is described in the supplementary section of Kraft et al. (13).

4. Results

4.1 Intracranial Pressure

The highest pressures existed in the frontal regions of the brain, while the pressures decreased along the sagittal plane in the posterior direction. The intracranial pressure results were dependent on the material properties assigned to the skin (figure 3), which vary largely in the literature. Previous validation studies with the model were done using a homogeneous skin/muscle/fat description (*17*). When using these material properties (*17*), the intracranial pressures exceeded the pressures measured at the surface of the forehead skin. When the material properties were altered to reflect (*26*), the intracranial pressure at the frontal lobe was approximately 60% less than the total pressure at the surface of the skin.
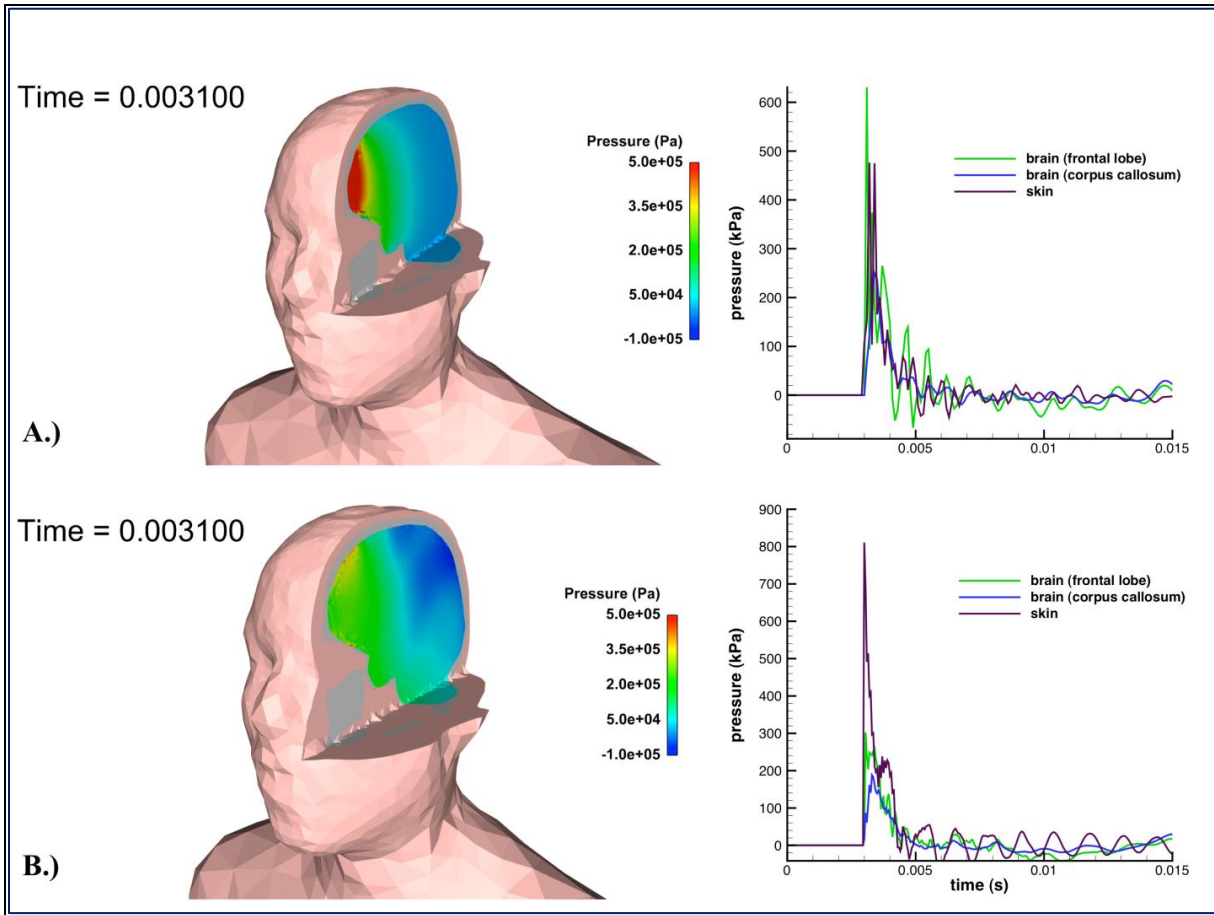

Figure 3. Transmitted pressure changes drastically with different material properties assigned to the skin. A.) Intracranial pressure using former skin/muscle/fat homogeneous material properties (K=1.67e7, ν =0.42); B.) Intracranial pressure using scalp material properties (K = 2.2e9, ν = 0.499).

Future efforts will focus on validation of the pressure response in a blast event, and utilize region-specific material properties for skin, muscle, and fat. In both simulations with different skin material properties, the pressure impulse from the blast wave ends within a few milliseconds after reaching the head, before any noticeable rotation of the head begins (figure 4).

4.2 Axonal Strain

The skull rotation angle was calculated from the axis created from the foramen magnum to the top of the cranial bone. The skull was assumed to be rigid in this calculation, since the maximum principal strains within the cranial bone were on the order of approximately $\times 10^{-4}$. A maximum cranial rotation angle of 5° was seen at 20 ms (approximately 17 ms after the arrival of the shock front). The rotation would increase in cases where the peak incident pressure and reflected pressure were larger; however, survivability at these levels becomes more uncertain, therefore axonal strains of a lower blast exposure (210-kPa incident pressure) were examined.

The largest axonal strains exceeded 0.17 (figure 5), and increased at the center of the brain throughout the progression of the simulation. Elements around the surface of the brain and near the ventricles also exhibited a large amount of axonal strain at later times. Axonal strain is not seen in the cerebellum because the original fiber tractography imaging did not include fiber directions for this region; therefore, this analysis can draw no conclusions regarding axonal strain in the cerebellum white matter.
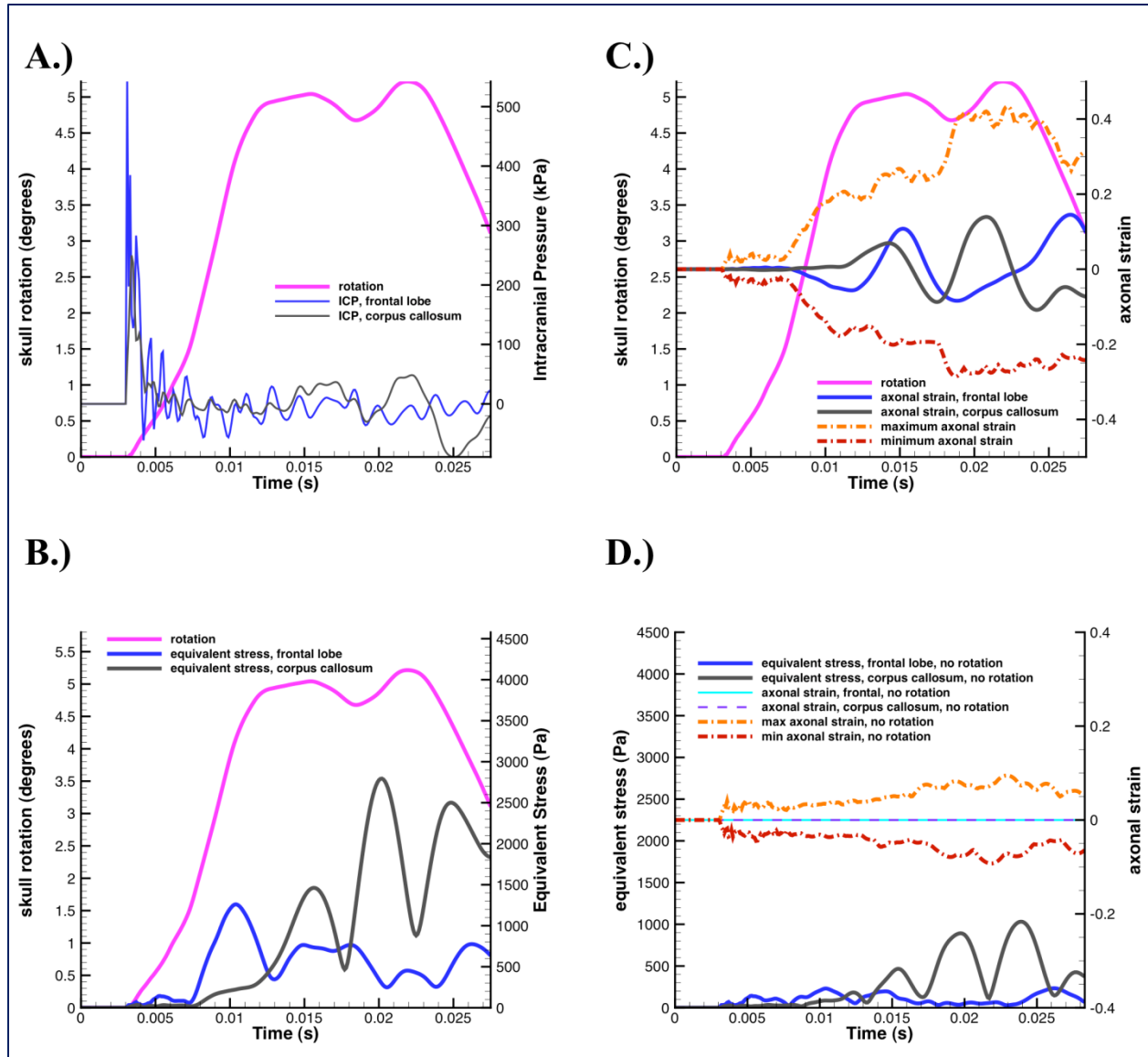
Figure 4. A.) Intracranial pressure plotted alongside rotation; B.) Equivalent stress plotted alongside head rotation; C.) Axonal strain plotted alongside head rotation; D.) Axonal strain and equivalent stress in the simulation with purely translational (no rotational) acceleration.

Figure 5. Top and side views of largest axonal strain values. Red elements experienced an axonal strain equal or greater than 0.17 in tension. Blue elements experienced a compressive strain of at least 0.17. The 0.12–0.17 strain range includes elements in both compression and tension.

4.3 Deviatoric Stress

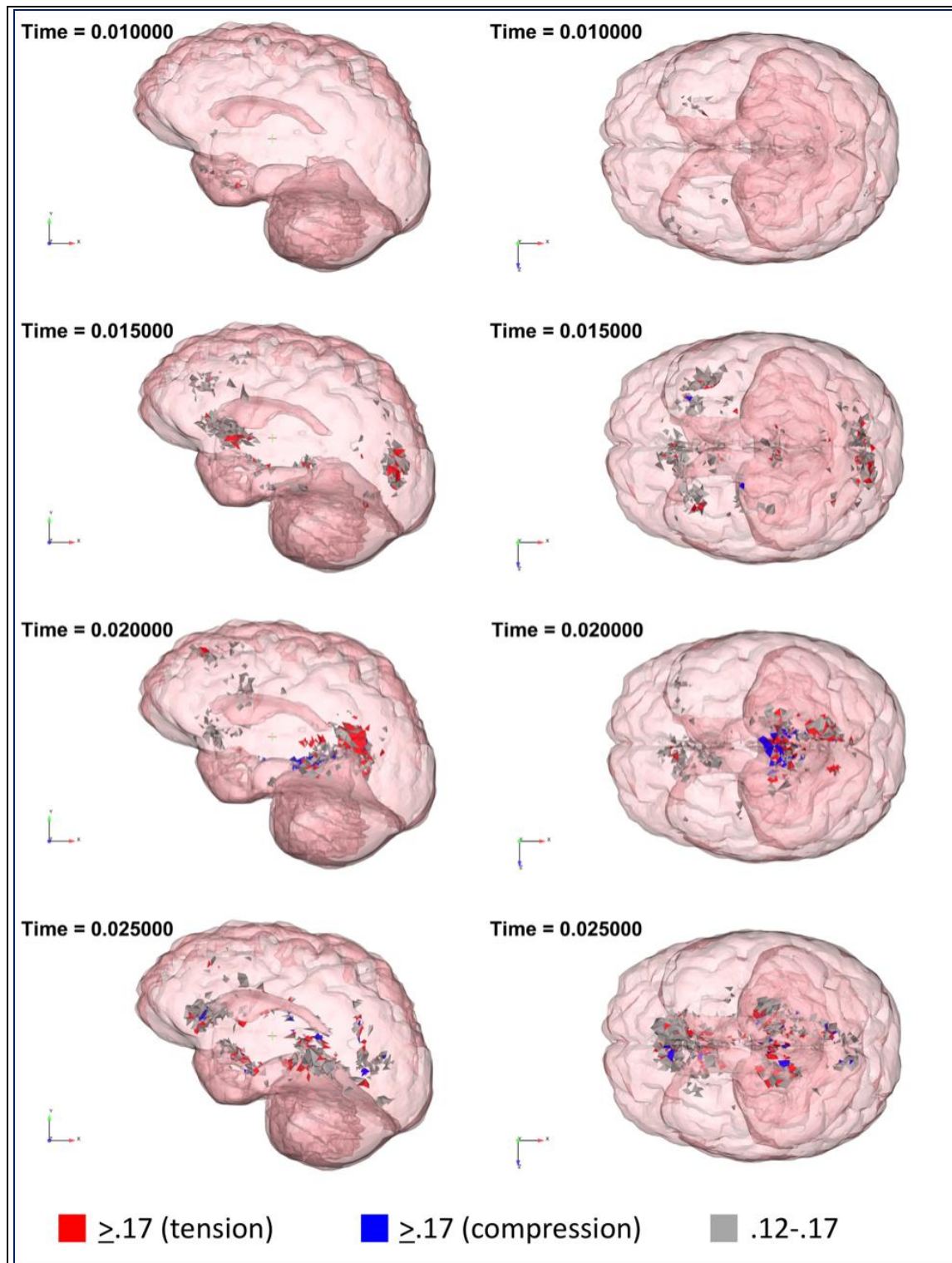The equivalent stress, which is a representative scalar derived from the deviatoric component of the stress tensor, is defined below:

$$\sigma_{vm} = \sqrt{\frac{1}{2}[(\sigma_{xx} - \sigma_{yy})^2 + (\sigma_{yy} - \sigma_{zz})^2 + (\sigma_{zz} - \sigma_{xx})^2 + 6(\sigma_{xy}^2 + \sigma_{yz}^2 + \sigma_{zx}^2)]} \qquad (5)$$

The equivalent stress is smaller in the beginning of the simulation, and gets larger towards the center of the brain at later times (figure 6). This is consistent with previous impact-loading scenarios showing spherically converging shear stress waves (*27*). The equivalent stress is smaller in the beginning of the simulation, and become largest around 15 ms after the arrival of the blast wave. Since the bulk modulus of brain tissue is orders of magnitude greater than the shear modulus, the propagation of distortional waves is much slower than the propagation of dilatational waves (*24*).

A second simulation was run with a free-boundary condition to allow for translational acceleration without rotational acceleration of the head (figure 4-D) to examine the response from nonrotational loading. The axonal strains were approximately zero in the same locations as the rotational simulation; however, low levels of axonal strains existed in other parts of the brain. The minimum and maximum axonal strains in the brain were still lower than most injury thresholds. A significant decrease was found in the deviatoric stress when no rotation was present.
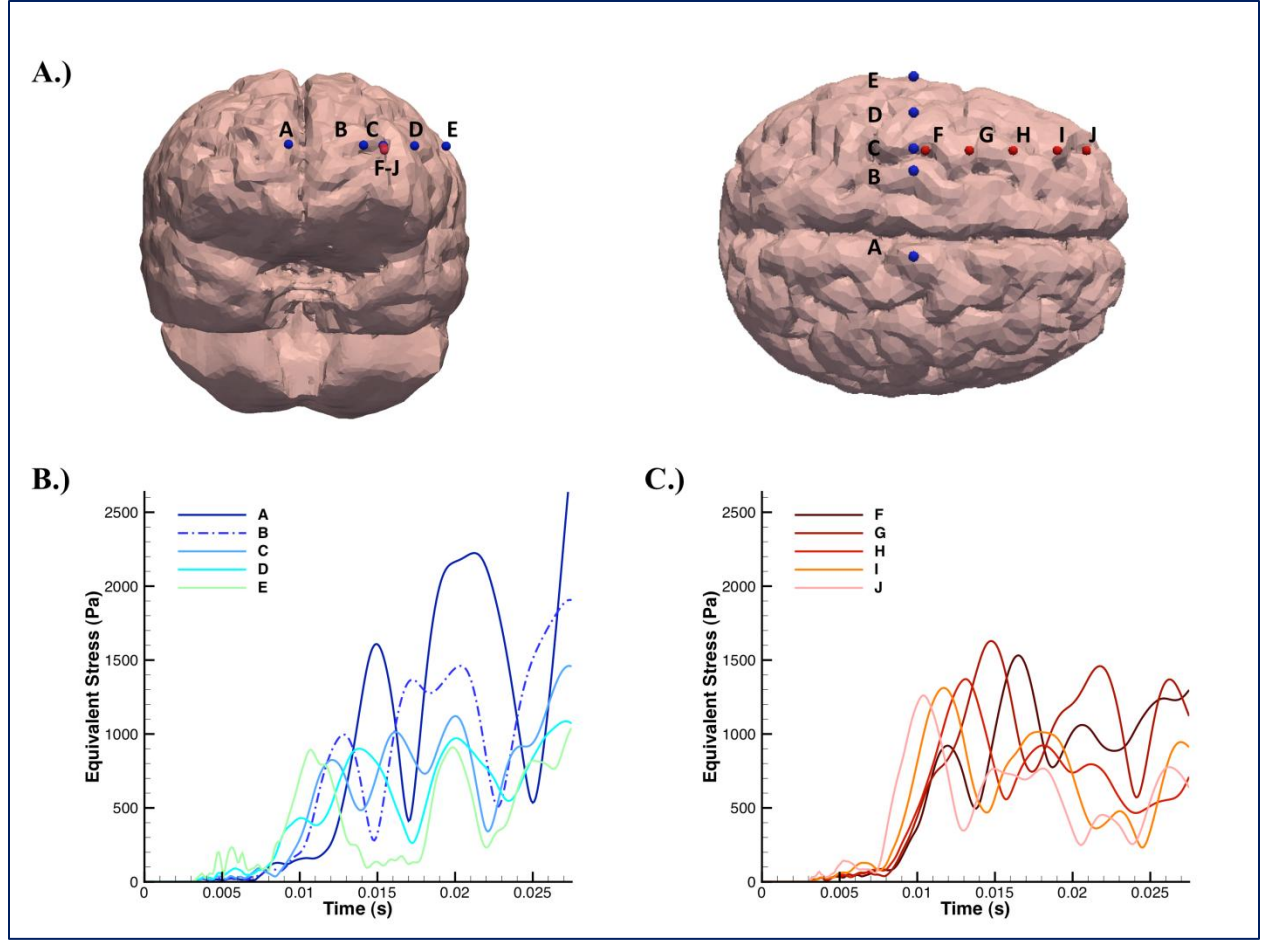
Figure 6. Shear stress behavior in transverse and sagittal planes. A.) Front and top view of data point locations; B.) Equivalent stress from the outside surface to the center of the brain (transverse plane); C.) Equivalent stress increases from the front surface of the brain to the center location (sagittal plane).

5. Discussion

5.1 Results from Simulations

The simulations show that fairly large pressures (100 kPa) will not produce large strains due to the high ratio of the bulk modulus to the shear modulus. A wide range of axonal injury thresholds exist in literature, ranging from 0.05 (*28*) to 0.21 (*29*). Meaney and Bain (*30*) have shown an electrophysiological impairment at axonal strain levels of 0.28 (liberal), 0.13 (conservative), and 0.18 (optimal) in tension. As shown in figure 4, the loading condition without head rotation did not create axonal strains beyond the conservative threshold for electrophysiological impairment.

The increased axonal strains towards the center of the brain could be caused by focusing of distortional waves towards the center, or because of the inhomogeneities of material properties in this region due to the close proximity of the brainstem, cerebellum, and cerebrospinal fluid. For the loading condition that allowed for rotational motion of the head, some locations of the brain exceeded this threshold and the maximum axonal strain found within the entire brain was almost twice the optimal threshold for electrophysiological impairment. In light of these findings, it may be important to examine the true strain—instead of the engineering strain—given the relatively large magnitudes of strains shown.

Zhang et al. (*31*) concluded that shear stress levels of 3.1–6.4 kPa in the thalamus could result in concussive injury and mild TBI. Our simulations have shown that the shear stresses are slightly below this threshold, although it is important to note that those conditions might have been reached if slightly higher shear properties were assigned to the brain tissue. Taylor and Ford (*7*) performed simulations of intracranial wave action over the first 2-ms after blast exposure, and found deviatoric stress levels close to 500 Pa, which is similar to the magnitude of deviatoric stress found in the simulation without rotation, although the deviatoric stress (*7*) appears within the first 2 ms of the simulation (*7*). This difference in the deviatoric response may be caused by differences in the material properties and the constitutive model used.

Blast wave injuries have historically been identified as (a) primary blast injury caused by the blast wave itself; (b) secondary injury caused by debris and fragmentation; (c) tertiary injury due to acceleration of the body by the blast wind and impacts into the ground or surrounding objects; and (d) flash burns or toxic gas inhalation resulting from the heat of the explosion (*32*). This raises the important question—what type of blast injury classification encompasses head rotation induced by blast-loading? Rotational acceleration of the head involves the acceleration of the body in tertiary injury; however, it lacks the impact event right after the body is thrown. It could also be classified as a primary injury, but this could be an inappropriate classification if primary injury is strictly related to the increased dilatational response.

5.2 Future Work

Although the post-blast brain tissue displacement presented in this study is similar to blunt impact results, future simulations must be compared to rotational head displacements found in high-rate blast-loading experiments. Recent experiments have been able to capture linear acceleration to a porcine head during blast-loading, but the current technology for angular rate sensors appropriate for blast-rate loading are limited and unable to yield meaningful results (*33*). In these simulations the dynamics of the head-neck system are important to the resulting biomechanical response and injury (*11*). Therefore, once validated, simulations like this would need to be reanalyzed with typical head-borne protective systems that might alter the inertial response.

Although active muscles have an effect on the response of the cervical spine in frontal impact scenarios, the muscle activation is believed to initiate at 74 ms (*34*), implying that it will not play a significant role in blast events, although this remains questionable without experimental validation. Also, cervical spine modeling has been extensively studied for automobile injury biomechanics, but extensive research has not been performed at higher rate loading regimes of blast events. The boundary condition of a fixed body below the neck is a rough approximation of the real articulation of the human body during a blast event. Future studies will examine the influence of translation and rotation of the human torso, which could also alter the amount of head rotation and strain within the brain.

The model used in this study contained ocular cavities in the facial bone, but lacked both openings on the sphenoid for the optic canals. This could potentially alter the soft-tissue pathway for pressure propagation into the brain in the frontal blast-load scenario presented in this study. It should also be noted that the model did not contain the sinus cavities, which would have also altered the pressure propagation into the brain.

The Lagrangian blast-loading model does not take account of any confinement or shadowing of intervening objects, nor does it account for possible changes in reflected pressure due to acceleration of the body. Therefore, a more accurate simulation, such as arbitrary Lagrangian-Eulerian or a 2-way coupling to capture the fluid-structure interaction, will need to be done in order to more accurately capture the pressure loading to which the body ultimately responds. For this analysis, the Lagrangian Presto Blast Function was used for computational efficiency and to achieve longer simulation times.

Ultimately, we hope to link our physics-based simulations with predictive clinical outcomes that may arise from TBI, such as neurodegenerative diseases. For example, recent studies have shown that chronic traumatic encephalopathy (CTE), a tau protein-linked neurodegenerative disease that leads to progressive deterioration of psychological and physical functions (*35*), is a major concern to military soldiers who experience a single or repetitive primary blast-loading to the head. Interestingly, head immobilization during blast exposure prevented CTE and functional deficits (*36*). Goldstein et al. (*36*) hypothesizes that the contribution of blast "wind" creates head accelerations that may be a primary factor leading to blast-related TBI and CTE.

6.   Conclusions

This preliminary study suggests that injurious levels of strain can be generated in the brain tissue from blast-loading. Although the peak pressure or impulse from the blast wave could play a major contribution to TBI, these simulation results indicate that mechanical loading, such as shear stresses and axonal strain, could concurrently contribute to TBI from blast events.

A 3-D FEM of the human head with transversely isotropic properties derived from Diffusion Weighted Imagaing data was used in a simulation of a blast event. Axonal strains were calculated to predict the extent of DAI in the brain during a blast event. It was found that the maximum axonal strain and shear stress attained their peak values about 10–15 ms after the initial contact of the blast wave. The time evolution of axonal strain indicated that axonal injuries increased as a consequence of head rotation.

7. References

1. Hyams, C. On the Signature Wound of the Iraq and Afghanistan Conflicts, Brain Injuries Range From the Loss of Coordination to Loss of Self, *USA Today*, 2005.

2. Desmoulin, G.; Dionne, J. P. Blast-Induced Neurotrauma: Surrogate Use, Loading Mechanisms, and Cellular Response. *J of Trauma,* **2009**, *67*, 1113–1122.

3. MacDonald, C., Johnson, A.; Cooper, D.; Malone, T.; Sorrell, J.; Shimony, J.; Parsons, M.; Snyder, A.; Raichle, M.; Fang, R.; Flaherty, S.; Russell, M.; Brody, D. Cerebellar White Matter Abnormalities following Primary Blast Injury in U.S. Military Personnel. *PLoSOne,* **2013**, *8* (2), 1–8.

4. Christman, C. W.; Grady, M. S.; Walker, S. A.; Holloway, K. L.; Povlishock, J. T. Ultrastructural Studies of Diffuse Axonal Injury in Humans. *J. Neurotrauma,* **1994**, *11* (2), 173–86.

5. Hagmann, P.; Jonasson L.; Maeder, P.; Thiran, J. P.; Wedeen, M. C.; Meuli, R. Understanding Diffusion MR Imaging Techniques: From Scalar Diffusion-Weighted Imaging to Diffusion Tensor Imaging and Beyond. *Radiographics,* **2006**, *46*, S205–S223.

6. Nyein, M. K.; Jason, A. M.; Yu, L.; Pita, C. M.; Joannopoulos, J. D.; Moore, D. F.; Radovitzky, R.A. In Silico Investigation of Intracranial Blast Mitigation With Relevance to Military Traumatic Brain Injury. *Proc Natl Acad Sci.,* **2010**, *107* (48), 427–433.

7. Taylor, P.; Ford, C. Simulation of Blast-Induced Early-Time Intracranial Wave Physics Leading to Traumatic Brain Injury. *Journal of Biomechanical Engineering,* **2009**, *131*, 061007–1.

8. Ganpule, S.; Alai, A.; Plougonven, E.; Chandra, N. Mechanics of Blast Loading on the Head Models in the Study of Traumatic Brain Injury Using Experimental and Computational Approaches. *Biomech and Modeling in Mechanbio,* **2012**, *12* (3), 511–31.

9. Gennarelli, T. A.; Thiebault, L. E.; Adams, J. H.; Graham, D. I.; Thompson, C. J.; Marcincin, R. P. Diffuse Axonal Injury and Traumatic Coma in the Primate. *Ann Neurol,* **1982**, *12* (6), 564–74.

10. Wright, R. M.; Ramesh, K. T. An Axonal Strain Injury Criterion for Traumatic Brain Injury. *Biomech ModelMechanobiol,* **2011**, *11*, 1–2, 245–260.

11. Wright, R. M.; Post, A.; Hoshizaki, B.; Ramesh, K. T. A Multiscale Computational Approach to Estimating Axonal Damage Under Inertial Loading of the Head. *J. Neurotrauma,* **2013**, *30* (2), 102–18.

12. Kraft, R. H.; Ziegler, K. High Rate Computational Brain Injury Biomechanics. *Proceedings of the ARL Ballistic Technology Workshop,* 2010.

13. Kraft, R.; McKee, P. J.; Dagro, A. M.; Grafton, S. Combining the Finite Element Method With Structural Connectome-Based Analysis for Modeling Neurotrauma: Connectome Neurotrauma Mechanics, *PLoS Comp. Bio.,* **2012**, *8* (8).

14. Kraft, R. H.; Dagro, A. M. *Design and Implementation of a Numerical Technique to Inform Anisotropic Hyperelastic Finite Element Models Using Diffusion-Weighted Imaging*; ARL-TR-5796; U.S. Army Research Laboratory: Aberdeen, MD, 2011.

15. Dohrmann, C. R.; Heinstein, M. W.; Jung, J.; Key, S. W.; Witkowski, W. R. Node-Based Uniform Strain Elements for Three-Node Triangular and Four-Node Tetrahedral Meshes. *Int. J. Numer. Meth. Eng*., **2000**, *47*, 549–1568.

16. Ho, J.; Kleiven, S. Can Sulci Protect the Brain From Traumatic Injury? *J. Biomech.*, **2009**, *13*, 2074–80.

17. Kleiven, S.; Hardy, W. N. Correlation of an FE Model of the Human Head With Local Brain Motion-Consquences for Injury Prediction. *Stapp Car Crash Journal,* **2002**, *46*, 123–44.

18. Prange, M. T.; Margulies, S. S. Regional, Directional, and Age-Dependent Properties of the Brain Undergoing Large Deformation. *Transactions of the ASME*, **2002**, *124*, 244–252.

19. Arbogast K. B.; Margulies, S. S. A Fiber-Reinforced Composite Model of the Viscoelastic Behavior of the Brainstem in Shear. *J. Biomech.*, **1999**, *32*, 865–870.

20. Mendis, K. Finite Element Modeling of the Brain to Establish Diffuse Axonal Injury Criteria, Ohio State University, OH, 1992.

21. Randers-Pehrson, G.; Bannister, K. A. *Airblast Loading Model for DYNA2D and DYNA3D*; ARL-TR-1310; U.S. Army Research Laboratory: Aberdeen Proving Ground, MD, 1997.

22. Bass, C. R.; Panzer, M. B.; Rafaels, K. A.; Wood, G.; Shridharani, J.; Capehart, B. Brain Injuries from Blast. *Annals of Biomedical Engineering,* **2012**, *40*, (1), 185–202.

23. Nahum, A. M.; Smith, R.; Ward, C. C. Intracranial Pressure Dynamics During Head Impact. *Proceedings of the 21st STAPP Car Crash Conference*, 1977.24.

24. Bradshaw, D. R. S.; Morfey, C. L. Pressure and Shear Response in Brain Injury Models, *Amsterdam Proceedings of the 17th Int. Technical Conference on the Enhanced Safety of Vehicles*, 2001.

25. Hardy, W. H.; Foster, C.; Mason, M.; Yang, K.; King, A.; Tashman, S. Investigation of Head Injury Mechanisms Using Neutral Density Technology and High-Speed Biplanar X-Ray. *45*th *Stapp Car Crash Journal,* **2001**, *45*, 337–368.

26. Panzer, M.; Myers B. S.; Capehart, B. P.; Bass, C. R. Development of a Finite Element Model for Blast Brain Injury and the Effects of CSF Cavitation. *Annals of Biomedical Engineering,* **2012**, *40* (7), 1530–44.27.

27. Chen, Y.; Ostoja-Starzewski, M. MRI-Based Finite Element Modeling of Head Trauma: Spherically Focusing Shear Waves. *Acta Mech.,* **2010**, *213*, 155–167.

28. Margulies, S. S.; Thibault, L. E. A Proposed Tolerance Criterion for Diffuse Axonal Injury in Man. *J Biomech*, **1992**, *25* (8), 917–23.

29. Kleiven, S. Predictors for Traumatic Brain Injuries Evaluated Through Accident Reconstructions. *Stapp Car Crash J.*, **2007**.

30. Bain, A.; Meaney, D. F. Tissue-Level Thresholds for Axonal Damage in an Experimental Model of Central Nervous System White Matter Injury. *J. Biomech Eng.,* **2000**, *122* (6), 615–22.

31. Zhang, L.; Yang, K. H.; King, A. I. A Proposed Injury Threshold for Mild Traumatic Brain Injury. *ASME J. Biomech Eng.*, **2004**, *126* (2), 1154–1172.

32. Owen-Smith, M. S. Explosive Blast Injury. *Med Bull U.S. Army Eur.*, **1981**, *38*, 36–43.

33. Sidharani, J. K.; Wood, G. W.; Panzer, M. B.; Capehart, B. C.; Nyein, M. K.; Radovitzky, R. A.; Bass, C. R. Porcine Head Response to Blast. *Frontiers in Neurology,* **2012**, 3 (70), 1–12.

34. Siegmund, G. P.; Myers, B. S.; Davis, M. B.; Bohnet, H. F.; Winkelstein, B. A. Mechanical Evidence of Cervical Facet Capsule Injury During Whiplash: A Cadaveric Study Using Combine Shear, Compression, and Extension Loading. *Spine 26*, **2001**, *26* (19), 2095–101.

35. McKee, A. C.; Cantu, R. C.; Nowinski, C. J.; Hedley-White, E. T.; Gavett, B. E.; Budson, A. E.; Santini, V. E.; Lee, H.; Kubilis, C. A.; Stern, R. A. Chronic Traumatic Encephalopathy in Athletes: Progressive Taopathy following Repetitive Head Injury. *J. Neuropathol Exp Neurol,* **2009**, 68 (7), 709–35.

36. Goldstein, L. E.; Fisher, A. M.; Tagge, C. A.; Zhang, X. L.; Velisek, L.; Sullivan, J. A.; Upreti, C.; Kracht, J. M.; Ericsson, M.; Wojnarowicz, M. W.; Goletiani, C. J.; Maglakelidze, G. M.; Casey, N.; Moncaster, J. A.; Minaeva, O.; Moir, R. D.; Nowinski, C. J.; Stern, R. A.; Cantu, R. C.; Geiling, J.; Blusztajn, J. K.; Wolozin, B. L.; Ikezu, T.; Stein, T. D.; Budson, A. E.; Kowall, N. W.; Chargin, D.; Sharon, A.; Saman, S.; Hall, G. F.; Moss, W. C.; Cleveland, R. O.; Tanzi, R. E.; Stanton, P. K.; McKee, A. C. Chronic Traumatic Encephalopathy in Blast-Exposed Military Veterans and a Blast Neurotrauma Mouse Model. *Science Translational Medicine*, **2012**, *4* (134), 1–16.

List of Symbols, Abbreviations, and Acronyms

ARL	U.S. Army Research Laboratory
bTBI	blast traumatic brain injury
CTE	chronic traumatic encephalopathy
DAI	Diffuse Axonal Injury
DSI	Dynamic Science, Inc.
DTI	Diffusion Tensor Imaging
FEM	finite element model
IED	improvised explosive device
m	meter
MR	magnetic resonance
MRI	magnetic resonance imaging
ms	milliseconds
NDT	neutral density target
3-D	three-dimensional
TBI	traumatic brain injury

19

NO. OF
COPIES ORGANIZATION

  4   DRDC VALCARTIER
(PDF)   K WILLIAMS
         A BOUAMOUL
         L MARTINEAU
         D NANDLALL

  1   DRDC TORONTO
(PDF)   C BURRELL

  1   IMPERIAL BLAST BIOMECHANICS
(PDF)   AND BIOPHYISCS GROUP
         DEPT OF BIOENGR
         S D MASOUROS

INTENTIONALLY LEFT BLANK.